RSC Advances

This is an *Accepted Manuscript*, which has been through the Royal Society of Chemistry peer review process and has been accepted for publication.

Accepted Manuscripts are published online shortly after acceptance, before technical editing, formatting and proof reading. Using this free service, authors can make their results available to the community, in citable form, before we publish the edited article. This *Accepted Manuscript* will be replaced by the edited, formatted and paginated article as soon as this is available.

You can find more information about *Accepted Manuscripts* in the Information for Authors.

Please note that technical editing may introduce minor changes to the text and/or graphics, which may alter content. The journal's standard Terms & Conditions and the Ethical guidelines still apply. In no event shall the Royal Society of Chemistry be held responsible for any errors or omissions in this *Accepted Manuscript* or any consequences arising from the use of any information it contains.

ROYAL SOCIETY OF CHEMISTRY

www.rsc.org/advances

Fabrication and excellently visible-light-driven photodegradation activity for antibiotics of $SrTiO_3$ nanocubes coated CdS microspheres heterojunction

Guoling Wu[a,b], Lisong Xiao[b], Wei Gu[b], Weidong Shi[b], Dayu Jiang[a,*], Chunbo Liu[b,*]

a College of Chemistry, Jilin Normal University, Siping, 136000, P. R. China

b School of Chemistry and Chemical Engineering, Jiangsu University, Xuefu Road 301, Zhenjiang, 212013, P. R. China

**Corresponding author: Tel.:+86 0511 8879 0187 fax.:+86 0511 8879 1108*

E-mail address: swd1978@ujs.edu.cn; liuchunbojsu@163.com

RSC Advances Accepted Manuscript

Abstract

Extending the light absorption range and facilitating the separation of photoinduced carriers are of effective strategy in the process of photocatalytic. An effective method is to construct the heterostructure. In this work, a new heterojunction $CdS/SrTiO_3$ was synthesized via two steps hydrothermal route and designed to decontaminate the hazardous wastewater containing antibiotics under visible light irradiation. Specially, the efficient photocatalytic performance of the composites could ascribe to the enhancement of visible light absorption efficiency and the efficient separation of the photoexcited carriers originating from the heterointerface. Furthermore, a plausible photocatalytic mechanism has been discussed in detail based on the trap experiments and ESR analysis results. $CdS/SrTiO_3$ heterojunction have a potential application prospect for purifying antibiotic pollutants in the environmental waste water because of its high efficiency and stability.

Keywords: $CdS/SrTiO_3$; Heterojunction; Antibiotics; Photodegradation; Universality

1. Introduction

At the present, the abuse of pharmaceuticals, especially antibiotics, in the wastewaters have caused a serious environmental problem worldwide owing to their high consumption. When these antibiotics are ingested by human and livestock, they are partially excreted from the body as either metabolites or unmodified parent compounds into environmental waters in the pharmaceutically active form, which may be a case of alarm over the aquatic ecosystems as well as the public health.[1-4] Therefore, the development of efficient treatments for eliminating antibiotics left in the ecological environment is an urgent task. Semiconductor photocatalysis has been considered an effective process in the mitigation of environmental questions resulted from the occurrence of organic contaminants in the environment using solar energy.[5-8] The unremitting efforts over the past forty years have made obvious achievements in semiconductor photocatalytic degradation fields, just as the literature reported

RSC Advances Accepted Manuscript

before.[9-11] However, most of the reports for applications in degrading organic pollutants mainly focused on degradation of a single contaminant. The hazardous wastewater usually contains multiple antibiotics pollutants. Therefore, exploiting the new photocatalysts not confined to a single contaminant is of high interest and has an important significance.

To date, the $SrTiO_3$ semiconductor has undoubtedly been proven to be one of the renowned photocatalysts due to the excellent chemical stability, non-toxicity, low cost and favorable optoelectronic properties, which is deemed to be a promising photocatalyst for water splitting, inactivating viruses and completely eliminating organic contaminants. [12-16] However, as a model ultraviolet (UV) photocatalyst similar to TiO_2, $SrTiO_3$ is particularly suitable for applications based on UV-light irradiation, which occupies only 4% of the incoming solar light spectrum on the earth. In order to push the absorption onset of $SrTiO_3$ toward longer wavelength that covers the largest proportion of the solar spectrum, strenuous efforts have been devoted, including doping, [17,18] suitable textural design, [19,20] and coupling with metal[21] or other semiconductor[22,23]. Among these, designing composite material with matched band-edges is an important and effective strategy because it facilitates the immigration and separation of photo-generated electrons and holes, leading to an improved overall efficiency. [24-26] Some composites of $SrTiO_3$ ($SrTiO_3/Fe_3O_4$,[27] $SrTiO_3/Cu_2O$,[28] $Ag_3PO_4/SrTiO_3$[29]) were also reported on the enhancement of the photocatalytic O_2 and H_2 production activity or organic pollutants elimination ability under visible light irradiation. Therefore, fabricating the newfangled composite heterostructure is a tempting method to sensitize $SrTiO_3$ with higher visible light absorption and electron migrating efficiency. CdS has been extensively researched as a common photocatalyst for its favorable band gap (2.42 eV), whose conduction band (CB) and valence band (VB) are both negative compared to those of $SrTiO_3$.[30-32] Thus, it is conjectured that the heterostructure constructed between CdS and $SrTiO_3$ not only extends the absorption of $SrTiO_3$ to the visible light region but may also boost electron transmissions from the CB of CdS to that of $SrTiO_3$. Such a result exhibits great achievements to the advancement of photocatalytic activity. To our knowledge,

RSC Advances Accepted Manuscript

no prior works concerning the employment of $CdS/SrTiO_3$ heterojunction as an effective photocatalyst for degrading antibiotics have been reported to date.

Inspired by the above, we herein fabricated the $CdS/SrTiO_3$ heterojunction via the surface modification strategy using a two-step simple hydrothermal method for the first time. It demonstrated the superior photocatalytic activity in the degrading five kinds of antibiotics under visible light irradiation, such as ciprofloxacin (CIP), enrofloxacin hydrochloride (ENR), oxytetracycline (OTC), danofloxancin mesylate (DAN) and levofloxacin (LEV) and so on. Specially, the effect of CdS microspheres content on the photocatalytic activity was evaluated and the appropriate content of CdS microspheres (60wt%) plays an essential role in improving synergetic effects on the transfer of the carriers. In addition, the stability of $CdS/SrTiO_3$ heterojunction photocatalysts was monitored by the circulation experiments. This work demonstrates that the $CdS/SrTiO_3$ heterostructures provide performance of highly efficient, stable, and reusable for potential application in waste water treatment.

2. Experimental

2.1. Materials

Titania TiO_2 (P25) powder was purchased from Degussa (Germany). $Sr(OH)_2{\cdot}8H_2O$, KOH, $Cd(CH_3COO)_2{\cdot}2H_2O$ and thiourea (CN_2H_4S) were purchased from Aladdin (Shanghai, China). All the reagents are analytically grade and used without further purification.

2.2. Preparation of photocatalyst

Pure phase $SrTiO_3$, with a particle size of approximately 50 nm, was synthesized by a hydrothermal method. In a typical synthesis, 3 mmol $Sr(OH)_2$ was dissolved in 35 mL of distilled water keeping vigorous stirring to form a suspension solution, to which 3.5 mmol of P25 was put into, and 2 g of KOH was finally added into the mixture keeping pH 13.0. After stirring for 30 min, the mixture was transferred into a 50 mL Teflon-lined stainless autoclave for hydrothermal treatment at 150°C for 72 h. The white precipitate was obtained by centrifugation and then washed with distilled water and ethanol until the pH reached 7 and afterward, it was dried overnight at 60°C. The

RSC Advances Accepted Manuscript

$SrTiO_3$/CdS heterostructures were synthesized by the hydrothermal method too. We take the $SrTiO_3$/CdS-60wt% as a model: 0.1835g of as-prepared $SrTiO_3$ nanocubes was dispersed into 50 mL of distilled water and ultrasonically treated for 10 min. Then 0.505g $Cd(CH_3COO)_2 \cdot 2H_2O$ and 0.288g CN_2H_4S (Cd^{2+}/S^{2-} = 1:2) were mixed and dissolved by stirring for 1 h. Subsequently, the mixture was loaded in a 100 mL Teflon-lined stainless steel autoclave. The autoclave was sealed and heated in a program-controlled oven at 180°C for 10 h and then air-cooled to room temperature. The resultant products were separated by centrifugation, washed with distilled water and ethanol, and dried in a vacuum at 60°C for one night. We have also conducted the hydrothermal method for the synthesis of pure CdS microspheres using the same method above in the absent of $SrTiO_3$, which is reported in literature.[32]

CdS/$SrTiO_3$ heterojunctions were obtained by simply adjusting the usage of CdS and were labeled as SC-x, in which x refers to the CdS loading amount (10 wt%, 40 wt%, 60 wt%, 70 wt% and 80 wt%).

2.3. Photocatalysts characterization

Powder X-ray diffraction (XRD) patterns were obtained with a D/MAX-2500 diffractometer (Rigaku, Japan) with the Cu Kα radiation from 10° to 80° with a step size of 0.02° at a scan rate of 5° min^{-1}. Transmission electron microscopy (TEM), high-resolution (HR-TEM) and high-angle annular dark-field scanning transmission electron microscopy (HAADF-STEM) were performed on JEM-2100 (HR) microscopes with a field-emission gun and the acceleration voltage for both microscopes was 200 kV. Scanning electron microscopy (SEM) and energy dispersive spectroscopy (EDS), have been used to characterization the samples. UV−vis absorption spectra of the samples were recorded with a Shimadzu UV-2500 spectrophotometer using $BaSO_4$ as reference. X-ray photoelectron spectroscopy (XPS) data of the samples were observed by a Thermo ESCALAB 250X (America) electron spectrometer using 150 W Al Kα radiations. Electron Spin Resonance (ESR) analysis was performed from a Bruker EPR A300-10/12 spectrometer.

RSC Advances Accepted Manuscript

2.4. Photocatalysts reaction

Photocatalytic activities of the as-prepared photocatalysts were estimated by degrading multiple antibiotics using a photochemical reactor under the visible light irradiation (250 W Xe lamp with a cut-off filter of 400 nm). Under such condition, the optical power density is 150 mW/cm^2 (CEL-NP2000). Firstly, take CIP for example. In each experiment, 100 mg photocatalyst was added into CIP aqueous solution (10 mg/L, 100 mL). Prior to irradiation, the suspensions were magnetically stirred in the dark for 30 min to achieve the absorption–desorption equilibrium between the photocatalysts and pollutants. During the degradation progress, 5 mL suspension was sampled in 20 min interval and centrifuged (10,000 rpm, 5 min) to remove the photocatalyst particles. The concentration of aqueous CIP was determined with a spectrometer by measuring the absorbance at 277 nm.[33] The photocatalytic degradation ratio (DR) was calculated by the following formula:

$$DR\% = 100\% - (A_i/A_0) \times 100\%$$

Where A_0 is the initial absorbance of CIP when reached absorption equilibrium, and A_i is the absorbance of degraded solution at the certain minutes.

Additionally, in order to verify the universality of as-prepared CdS/$SrTiO_3$ heterojunction, the degradation of the other four antibiotics, such as ENR, OTC, DAN and LEV were further estimated under visible light. The operational processes were the same with the CIP degradation. The concentrations of ENR, OTC, DAN and LEV was also monitored using an UV–vis spectrophotometer at the wavelength of 275 nm,[34] 355 nm,[35] 282 nm and 294 nm, respectively.

2.5. Photocurrent measurements

Photocurrent density was carried out in a prescriptive three-electrode system employed a Pt wire as the counter electrode, the samples as the working electrode and Ag/AgCl (saturated KCl) as reference electrode, respectively. Transparent conductive fluorine-doped tin oxide (FTO) coated glass with the size of 10 mm × 30 mm × 2 mm were used as substrates for the deposition of the films. Before deposition of photocatalysts onto FTO coated glass, the substrate was cleaned in an ultrasonic bath using acetone, chloroform, ethanol and distilled water each for 30 min. The

RSC Advances Accepted Manuscript

as-prepared photocatalysts film electrodes on FTO coated glass served as the working electrode. The working electrode was prepared by a simple casting method as follows: 0.3 g of each sample and 0.02 g of polyethylene glycol were dispersed into 3 mL of ethanol and 0.03 mL oleic acid to form the slurry.[36] Then the slurry was dropped onto FTO coated glass via drop-casting method. The electrodes were then dried in a tube furnace, and calcined at 350°C for 2h under flow of N_2 gas. The photocurrent was collected and measured via electron shuttles on an inert Pt electrode immersed in electrolytic tank with 0.5 M Na_2SO_4 aqueous solution at a 0.5 V potential bias under a 300 W Xenon lamp exposure.

3. Results and discussion

3.1. Structural characterization of as-prepared photocatalysts

X-ray diffraction (XRD) was used to investigate the phase composition, purity, and crystallinity of the resulting products. Fig. 1a shows the XRD patterns of CdS, CdS/$SrTiO_3$, and $SrTiO_3$. Six diffraction peaks appear at 2θ = 22.8°, 32.4°, 40°, 46.5°, 57.8°, 67.8° and 77.2°, respectively, which coincide with the diffraction patterns of $SrTiO_3$ (ICDD PDF#84-0444). The major diffraction peaks at 2θ values of 24.8°, 26.5°, 28.2°, 43.7° and 52.9° are indexed to (100), (002), (101), (110) and (201) crystallographic planes of CdS (ICDD PDF#75-2306), respectively. The XRD pattern of CdS/$SrTiO_3$ composite is similar to the $SrTiO_3$ and CdS, which shows a combination of $SrTiO_3$ and CdS, and rules out the possibility of other impurity phases, indicating successful construction of heterojunction. The elemental analysis of the CdS/$SrTiO_3$ heterojunction was carried out by acquiring EDS, as shown in Fig. 1b, from which Cd, S, Sr, O and Ti elements can be directly observed.

RSC Advances Accepted Manuscript

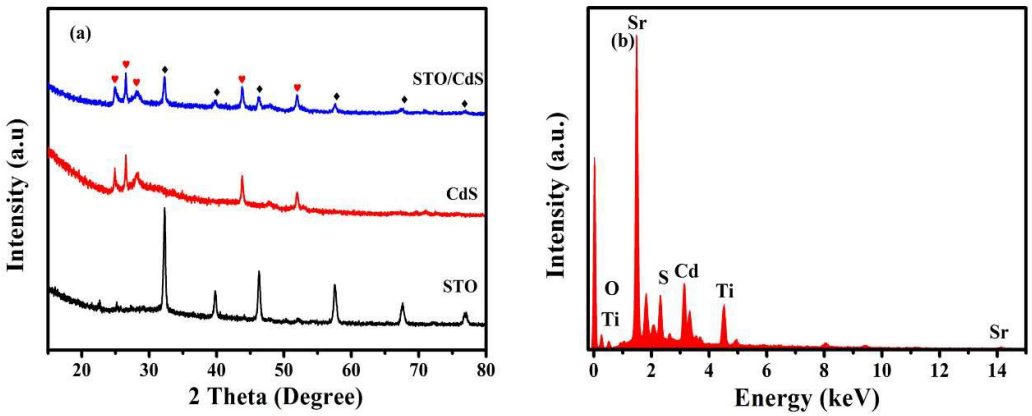

Fig. 1 (a) XRD patterns of $SrTiO_3$ (STO), CdS and CdS/$SrTiO_3$; (b) EDS spectrum of SC-60

To investigate the surface morphology and particle size of the representative photocatalysts, the typical electron microscope images were performed. From the SEM image in Fig. 2a, it is clear that the pure CdS possesses uniform-sized microspheres with the overall size of approximately 300 nm in diameter. The TEM image in Fig. 2b shows that pure $SrTiO_3$ particles display high uniform and regular cubes with diameters in the range of 20−50 nm. To provide better investigating into the interface contact features of the as-prepared heterojunction, TEM and HR-TEM were carried out. From Fig. 2c, it is found that the $SrTiO_3$ nanocubes grow obviously on the CdS microspheres. The TEM image in Fig. 2d further demonstrates the tight connection between $SrTiO_3$ nanocubes and CdS microspheres, which is beneficial to the interparticle photo-induced carriers transfer. The detailed nano-junction structure is displayed via the typical HR-TEM image in Fig. 2d. The d-spacings of 0.299 and 0.289 nm match the (101) lattice plane of CdS and the (110) lattice plane of $SrTiO_3$, respectively. Fig. 3 displays HAADF-STEM of CdS/$SrTiO_3$ heterojunction to identify the composition and element distribution. Elements corresponding to O, Sr, Ti, Cd and S are observed, which are derived from $SrTiO_3$ and CdS, respectively. Besides, the results of the HAADF-STEM elemental maps also confirm the $SrTiO_3$ nanocubes are uniformly distributed on the surface of the CdS microspheres.

RSC Advances Accepted Manuscript

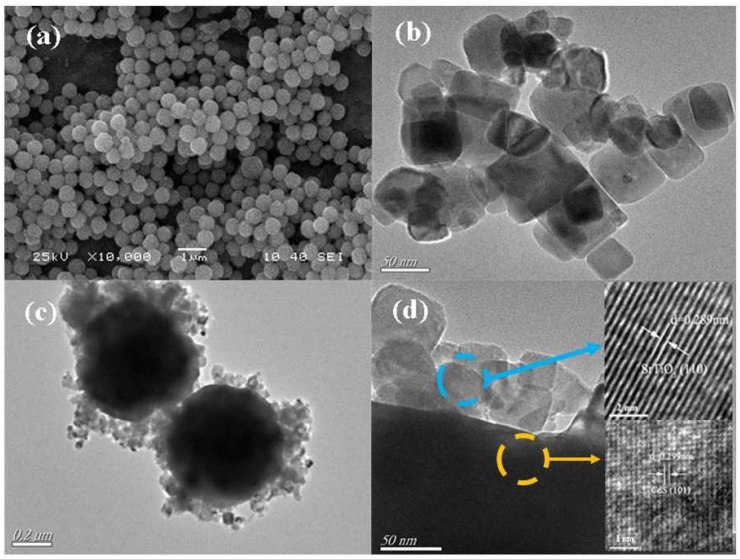

Fig. 2 (a) SEM images of pure CdS; TEM images of (b) pure $SrTiO_3$, (c) SC-60 and (d) HRTEM images of SC-60.

RSC Advances Accepted Manuscript

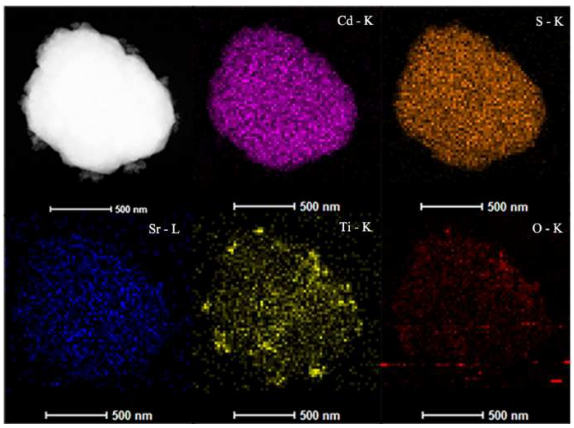

Fig. 3 HADDF–STEM image of the SC-60 sample with maps of Cd–K, S–K, Sr–L, Ti–K and O–K.

The XPS spectra were recorded to provide the surface compositions and chemical state present in the $CdS/SrTiO_3$ heterojunction. The full survey spectrum (Fig. 4a) shows that the sample is composed of Cd, S, Sr, Ti and O elements, and no other impurities are detected, which agrees well with the results of EDS. Fig. 4b shows the high-resolution Cd 3d XPS spectrum of $CdS/SrTiO_3$ heterojunction, the peaks occurred at 405.9 eV and 412.9 eV are ascribed to Cd $3d_{3/2}$ according to the standard database, which can be attributed to the Cd^{2+} in CdS. From Fig. 4c, it can be found that the peak of binding energy for S $2p_{3/2}$ is located at 161.5 eV, which is assigned to S^{2-} ions. Two strong peaks centered at 133.2 eV and 134.9 eV are observed in Fig. 4d, belonging to Sr $3d_{5/2}$ and Sr $3d_{3/2}$ states, respectively, which implies that the main elemental chemical states are divalent and bands with titanates.[37] From the XPS spectrum of Ti 2p shown in Fig. 4e, the banding energy of Ti $2p_{3/2}$ and Ti $2p_{1/2}$ peaks at 458.4 eV and 463.6 eV are assigned to Ti^{4+}, which results from $SrTiO_3$. The XPS spectrum of O 1s locates at the binding energies of 529.2 eV. All above results manifest that $CdS/SrTiO_3$ heterojunction is successfully prepared by the two steps hydrothermal route.

RSC Advances Accepted Manuscript

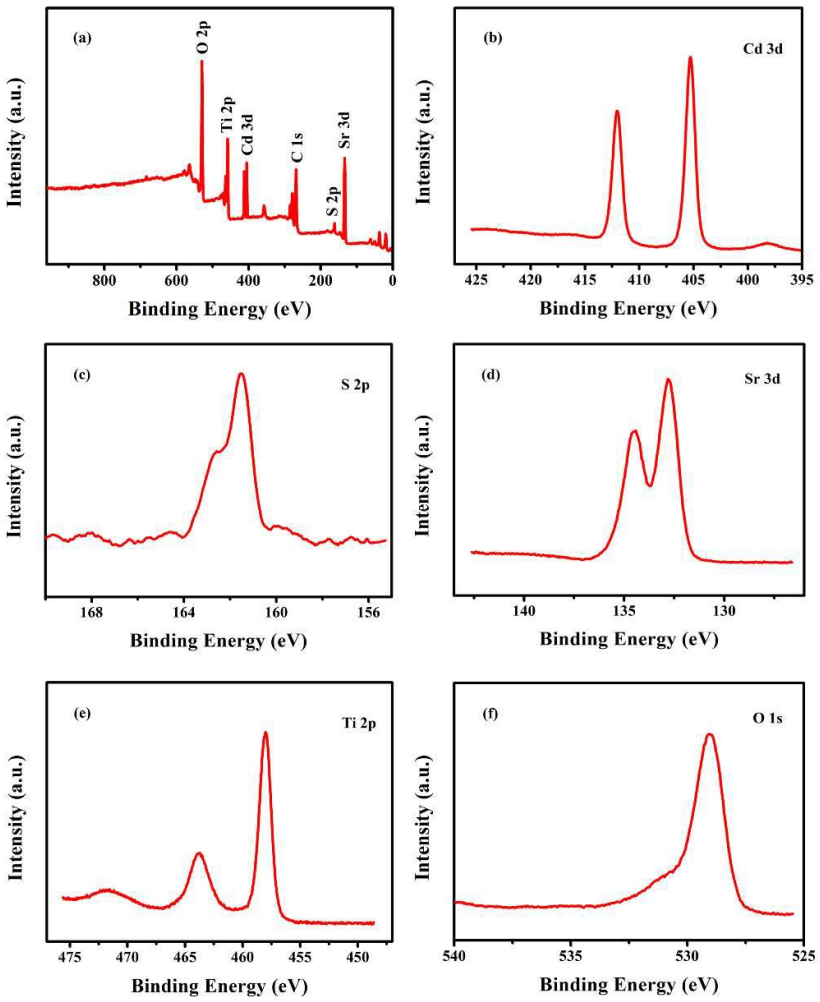

Fig. 4 XPS spectra of SC-60: (a) survey spectrum, (b) Cd 3d, (c) S 2p, (d) Sr 3d, (e) Ti 2p and (f) O 1s.

3.2. UV–vis adsorption of as-prepared photocatalysts

The UV−vis absorption spectra of as-synthesized samples in the pressed disk form were recorded on a Shimadzu UV-2500 spectrophotometer equipped with an integrating sphere assembly, over a wavelength range of 200−700 nm employing $BaSO_4$ as a reflectance standard. The pressed disk is compose by $BaSO_4$ powders and as-synthesized samples: $BaSO_4$ powders were flatted on the diffusion reflective cell, went its level planish again, 50mg as-synthesized samples were planished on the center of diffusion reflective cell. The light absorption properties of the prepared $SrTiO_3$, CdS and CdS/$SrTiO_3$ heterojunction were shown in Fig. 5. The spectrum of pure $SrTiO_3$ has a sharp absorption edge at ~380 nm, corresponding to the band gap

RSC Advances Accepted Manuscript

energy of 3.2 eV. The absorption spectrum of CdS indicates that it can absorb visible light with an absorption edge at ~580 nm. Therefore, in contrast to CdS and $SrTiO_3$, the absorption characteristic of CdS/$SrTiO_3$ heterojunction exhibits a little difference with that of them, which is attributed to the interfacial interaction between the $SrTiO_3$ and CdS and the photosensitizing effect of the incorporated CdS microspheres.[38]

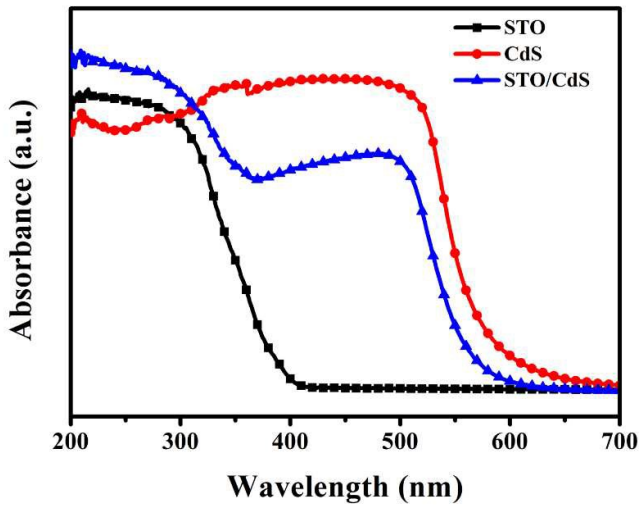

Fig. 5 UV–vis absorption spectra of the $SrTiO_3$, CdS and SC-60.

3.3. Photocatalytic activity and the stability of as-prepared photocatalysts

For elucidating the photocatalytic activities of the as-prepared samples on the antibiotics degradation, we performed the investigation of removing CIP as a model pollutant under visible light irradiation (λ> 420 nm) in 120 min, and the results are shown in Fig. 6a. There are 7 degradation curves in Fig. 6a, the vertical coordinates represented as degradation ratios, simply "DRs" for short. The CIP degradation rate of bare $SrTiO_3$ nanocubes is inappreciable because it can only be excited by UV light. In addition, the pure CdS microspheres reveal feeble photocatalytic performance for removing CIP (degradation rate of ~44.3%), which may be attributed to the high recombination rate of the photo-generated electrons and holes. However, the performance of CdS/$SrTiO_3$ heterojunction, by contrast, exhibits a remarkable enhancement for degrading CIP because of the enhanced charge separation efficiency resulting from its heterojunction structure. This based on the fact that CdS-sensitized

RSC Advances Accepted Manuscript

semiconductor composites can shuttle the photoexcited electrons from the CB of CdS to the CB of $SrTiO_3$,[38] which facilitates separation of electrons and holes, thus improving the degradation of CIP. Interestingly, Fig. 6b shows the activity of CdS/$SrTiO_3$ heterojunction for degrading CIP is enhanced rapidly with increasing content of CdS and then gradually decreased with further loading. When the content of CdS increases up to 60 wt% (SC-60), the degradation rate of CIP reaches to ~93.7%. It demonstrates that the CdS loading amount forcefully affects the photocatalytic activity.

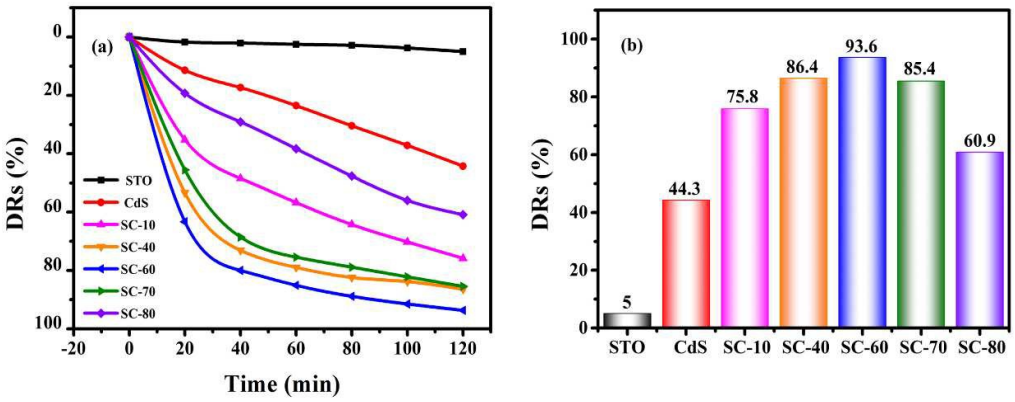

Fig. 6 Photocatalytic activity towards the degradation of CIP with as-prepared samples under visible light irradiation.

Considering the complexity of the practical wastewater, another four typical antibiotics of ENR, OTC, DFM and LEV were selected as the target pollutants for further evaluating photocatalytic activity of the SC-60 heterojunction. As shown in Fig. 7, the SC-60 heterojunction exhibits high photocatalytic activity for ENR, OTC, DAN and LEV mineralization (91.1%, 90.3%, 91.5% and 88.6%) under visible light irradiation, which is similar to degradation rate of CIP (93.7%). The results reveal that the CdS/$SrTiO_3$ heterojunction displays excellent visible-light-driven photocatalytic activity and can be a promising candidate for application in environmental purification.

RSC Advances Accepted Manuscript

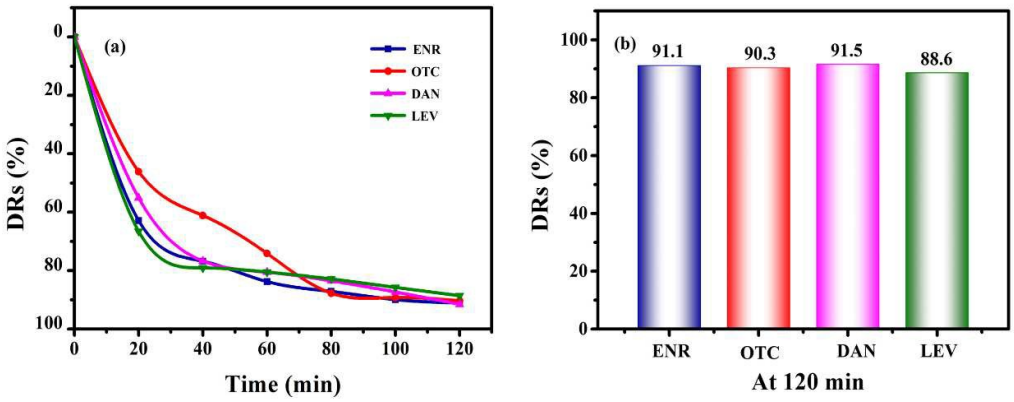

Fig. 7 The photodegradation performance of SC-60 sample for ENR, OTC, DAN and LEV degradation under visible light irradiation.

The reusability and stability of the photocatalyst are also of paramount importance to the practical application. To evaluate the stability of the photocatalytic performance of the SC-60 heterojunction, five consecutive cycles photocatalytic degradation of CIP were performed, using the same photocatalyst and a fresh CIP solution in each time. The results of the cycling experiments are depicted in Fig. 8. It exhibits that the photocatalytic activity of SC-60 heterojunction has a tiny deactivation in the photodegradation of CIP, which may originate from the unavoidable loss of the photocatalyst by centrifugation. Furthermore, the stability was detected by using XRD of the photocatalyst before and after the photocatalytic recycles. As shown in Fig. 8b, the XRD diffraction patterns of $CdS/SrTiO_3$ heterojunction have almost no change after photocatalytic cycles, implying that $CdS/SrTiO_3$ heterojunction is photostable and photocorrosion resistant.[39] Hence, $CdS/SrTiO_3$ heterojunction may serve as one of the promising candidates for application in purification of antibiotic waste water.

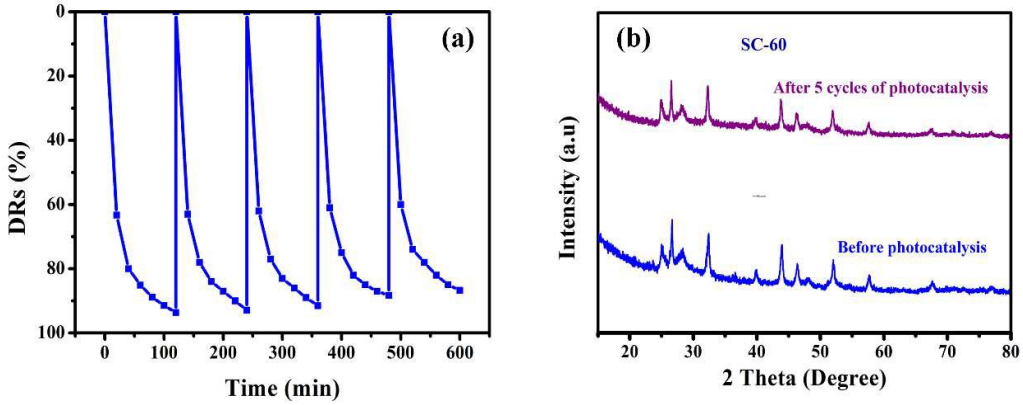

Fig. 8 (a) Five reaction cycles for the phtotcatalytic degradation of CIP by SC-60, and (b) XRD patterns of SC-60 before and after photocatalytic reaction.

RSC Advances Accepted Manuscript

3.4. Photoelectrochemical properties of as-prepared photocatalysts

The separation efficiency of excited electrons and holes for CdS/$SrTiO_3$ heterojunction can be validated by photocurrent under a 300 W Xenon lamp irradiation. Considering the several on–off cycles irradiation of transient photocurrent responses over the as-prepared electrodes, we have utilized photocurrent results to probe into the fate of photo-generated carriers.[40] The higher photocurrent density delegates enhanced transport and separation efficiency of the photo-generated carriers.[41] As delineated in Fig. 9, the photocurrent density of CdS/$SrTiO_3$ heterojunction is significantly higher than that of bare CdS, manifesting that it has more effective to separate the electron-hole pairs.[42,43] In addition, the optimum loading amount of CdS microspheres with 60 wt% exhibits the highest photocurrent density, indicating the remarkable reduction in recombination of photogenerated electrons and holes, which is consistent with its superior photocatalytic activity.

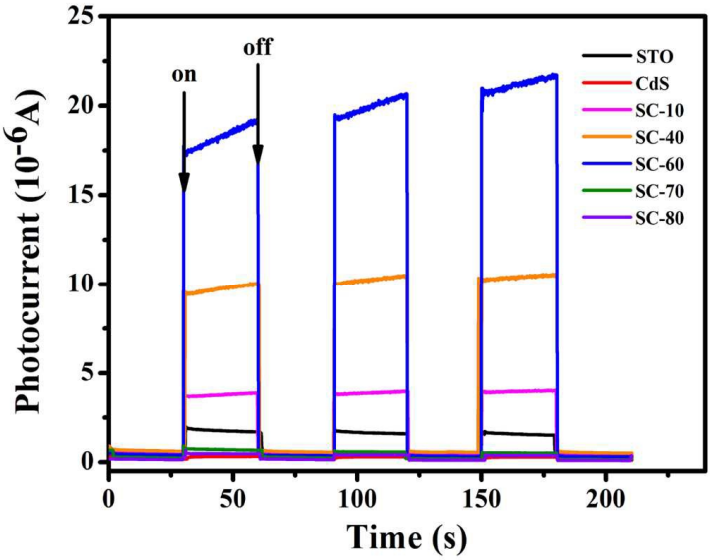

Fig. 9 Transient photocurrent response for the as-prepared samples.

3.5. Photocatalytic mechanism

To explore the mechanism of photocatalytic degradation of CIP utilizing SC-60 heterojunction photocatalyst, a series of quenchers were performed to determine the

RSC Advances Accepted Manuscript

dominant oxidative species in the photocatalytic process, namely, adding benzoquinone (BQ), isopropanol (IPA), $AgNO_3$ and triethanolamine (TEA) as a scavenger for $\bullet O_2^-$,[44,45] $\bullet OH$,[46] e^- [47,48] and h^+,[49] respectively. Fig. 10 presents degradation kinetic curves of CIP over SC-60 heterojunction under the different conditions. It is obviously shown that when the $AgNO_3$ (e^- scavenger) and BQ ($\bullet O_2^-$ scavenger) are added, respectively, the photocatalytic degradations of CIP are significantly inhibited, which confirms the paramount role of e^- and $\bullet O_2^-$ in the reaction process. Furthermore, the addition of IPA ($\bullet$OH scavenger) only leads to a small change in the photocatalytic degradation of CIP, indicating the contribution of $\bullet$OH radicals is secondary. However, the addition of TEA (h^+ scavenger) is used to remove h^+ bound to the surface, which only results in a tiny decrease in the photodegradation of CIP. Through the comparison, the importance of the activated species follows the order: $\bullet O_2^-$ >$\bullet$OH > h^+. In addition, based on the band gap positions, the CB and VB edge potentials of $SrTiO_3$ were defined at −0.4 eV and 2.8 eV and those of CdS are -0.52 eV and 1.88 eV, respectively.[38,50] The reduction potential of $O_2/\bullet O_2^-$ and $\bullet OH/H_2O$ is −0.33 eV and 2.7 eV (versus NHE), respectively. [51, 52] Thus, under the visible light irradiation, the electrons in CB of CdS will transfer into that of $SrTiO_3$ through the interface of $CdS/SrTiO_3$ heterojunction, which can afford to trap molecular oxygen to generate $\bullet O^{2-}$ and transform into some $\bullet$OH. By contrast, $\bullet O_2^-$ and $\bullet$OH are infeasible to be generated from CB of CdS directly. In addition, the holes play a small part in degrading CIP, which may result from the low potential of VB of CdS with the weak oxidation ability of the generated holes. Eventually, we can conclude that the degradation of CIP over SC-60 heterojunction is driven mainly by the participation of $\bullet O_2^-$, secondary by $\bullet$OH, and to a lesser extent by the contribution of h^+.

RSC Advances Accepted Manuscript

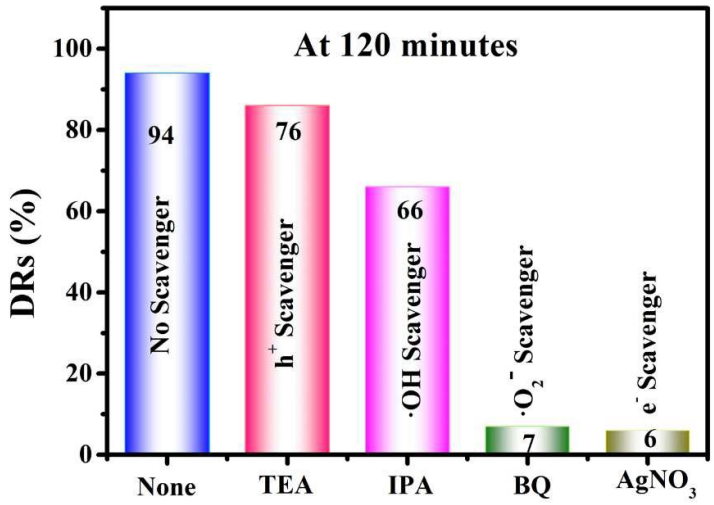

Fig. 10 Photocatalytic degradation of CIP with different radical scavengers over SC-60 under the visible light irradiation.

To further verify the generation of radicals ($\bullet O_2^-$ and $\bullet$OH), the ESR (Electron Spin Resonance) of SC-60 heterojunction was proceeded using dimethyl pyridine N-oxide (DMPO) as trapping agent. Before the measurement, the samples (5 mg) and DMPO (30 μL) were dispersed in deionized water and methanol, respectively. The former was used to detect the hydroxyl radicals (DMPO-$\bullet$OH), and the latter was used to detect the superoxide radicals (DMPO- $\bullet O_2^-$).[48,53] We have conducted the same procedure of pure CdS microspheres for comparison. As shown in Fig. 11, ESR signals of $\bullet O_2^-$and$\bullet$OH were detected at the same condition, and the signals intensity of the DMPO- $\bullet O_2^-$ are stronger than of the DMPO-$\bullet$OH for SC-60 heterojunction, indicating that the $\bullet O_2^-$ plays a leading role in the degrading CIP process, which is consistent with the previous trapping experiments. Besides, the signal intensities both DMPO- $\bullet O_2^-$and DMPO-$\bullet$OH of the pure CdS microspheres are weaker than SC-60 heterojunction. Herein, we may safely draw the conclusion that the CdS/$SrTiO_3$ heterojunction can be conducive to accelerate the electron transport and separation.

RSC Advances Accepted Manuscript

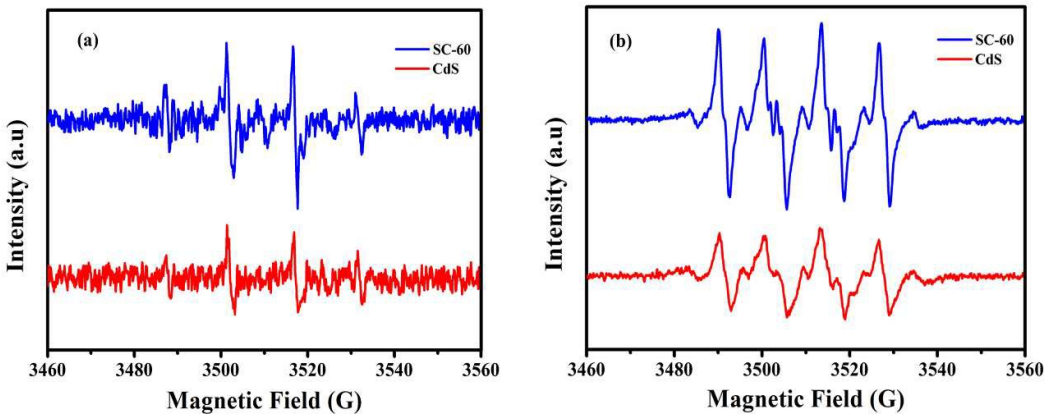

Fig. 11 DMPO spin-trapping ESR spectra of CdS and SC-60 for (a) DMPO-•OH and (b) DMPO-•O_2^- irradiated for 90 s.

Based on the above findings from the active species trapping experimental results and ESR analysis, a possible mechanism for the degradation of CIP over SC-60 heterojunction was presented in Scheme 1. Under the visible light irradiation, CdS in SC-60 heterojunction can be excited to form electron–hole pairs. Simultaneously, photoexcited electrons in the CB of CdS can fleetly transfer to CB of $SrTiO_3$. The electrons then diffuse to the surface of $SrTiO_3$ to activate molecular oxygen to form •O_2^- and efficeiently enhance the separation of charge carriers. A major of •O_2^- are directly involved in the oxidation of CIP. A fraction of the formed •O_2^- unceasingly result in the generation of •OH, which plays an assistant role in the photocatalytic degradation of CIP. The generated holes are released to the surface of photocatalysts to participate in the degradation of CIP to some extent. The possible photocatalytic reaction process can be expressed as follows:

$CdS + hv \rightarrow CdS\ (e^-_{CB} + h^+_{VB})$

$CdS\ e^-_{CB} + SrTiO_3 \rightarrow CdS + SrTiO_3\ (e^-_{CB})$

$SrTiO_3\ (e^-_{CB}) + O_2 \rightarrow SrTiO_3 + \bullet O_2^-$

$\bullet O_2^- + 2H_2O \rightarrow 2\bullet OH + H_2O_2$

$H_2O_2 \rightarrow 2\bullet OH$

$\bullet O_2^- + CIP \rightarrow$ Degraded products

$\bullet OH + CIP \rightarrow$ Degraded products

$CdS\ (h^+) + CIP \rightarrow$ Degraded products

RSC Advances Accepted Manuscript

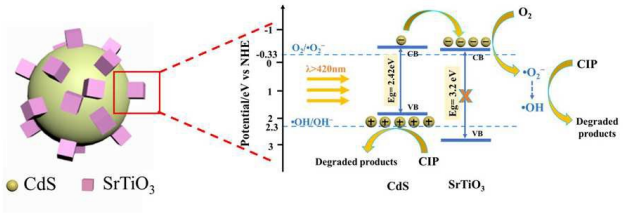

Scheme 1 Proposed reaction mechanisms for CIP degradation over SC-60 photocatalysts under visible light.

4. Conclusions

In this paper, the CdS/$SrTiO_3$ heterojunction is obtained by surface modification of $SrTiO_3$ nanocubes on CdS microspheres via two steps hydrothermal process. It shows improved photocatalytic activity for removing CIP pollutants under visible light irradiation, which is mainly ascribed to the heterostructure enhancing the separation efficiency of electrons and holes. Moreover, a possible photocatalytic mechanism is determined, confirming that $\bullet O_2^-$ radicals are the dominant active species to degrade CIP, and •OH radicals plays an assistant role in the photocatalytic degradation process of CIP. It is worth noting that CdS/$SrTiO_3$ heterostructure is no longer confined to degradation single CIP, which also exhibits universality for removing many kinds of antibiotics, such as ENR, OTC, DAN and LEV etc. This work provides an effective way to remove antibiotic pollutants in the environmental waste water owing to the high efficiency and stability of our obtained CdS/$SrTiO_3$ heterojunction.

Acknowledgements

We gratefully acknowledge the financial support of the National Natural Science Foundation of China (21546006, 21276116, and 21477050), Excellent Youth Foundation of Jiangsu Scientific Committee (BK20140011), Chinese-German Cooperation Research Project (GZ1091). Henry Fok Education Foundation (141068) and Six Talents Peak Project in Jiangsu Province (XCL-025). The Start-Up Foundation of Jiangsu University (11jdg104) and the Natural Science Foundation of Jiangsu Province (BK2012701).

References

1 S.E. Jørgensen, B. Halling-Sørensen, *Chemosphere*, 2000, **40,** 691.

RSC Advances Accepted Manuscript

2 A. Alighardashi, D. Pandolfi, O. Potier, M.N. Pons, *J. Hazard Mater.*, 2009, **72,**685.

3 S.D. Richardson, T.A. Ternes, *Anal. Chem.*, 2011, **83,** 4614.

4 D.A. Keane, K.G. McGuigan, P.F. Ibáñez, M.I. Polo-López, J.A. Byrne, P.S.M. Dunlop, K. O'Shea, D.D. Dionysiou, S.C. Pillai, *Catal. Sci. Technol.*, 2014, **4,** 1211.

5 H. Wang, L. Zhang, Z. Chen, J. Hu, S. Li, Z. Wang, J. Liu, X. Wang, *Chem. Soc. Rev.*, 2014, **43,** 5234.

6 S.Y. Reece, J.A. Hamel, K. Sung, T.D. Jarvi, A.J. Esswein, J.J.H. Pijpers, D.G. Nocera, *Science*, 2011, **334,** 645.

7 H. Tong, S. Ouyang, Y. Bi, N. Umezawa, M. Oshikiri, J. Ye, *Adv. Mater.*, 2012, **24,** 229.

8 M.R. Hoffmann, S.T. Martin, W. Choi, D.W. Bahnemannt, *Chem. Rev.*, 1995, **95,** 69.

9 J. Tiana, Y.H. Leng, Z.H. Zhao, Y. Xia, Y.H. Sang, P. Hao, J. Zhan, M.C. Li, H. Liu, *Nano Energy*, 2015, **11,** 419–427.

10 G.G. Bessegato, J.C. Cardoso, B.F. Silva, M.V.B. Zanoni, *Appl. Catal., B*, 2016, **80,** 161.

11 W.Y. Lu, T.F. Xu, Y. Wang, H.G. Hu, N. Li, X.M. Jiang, W.X. Chen, *Appl. Catal., B*, 2016, **80,** 20.

12 S. Ouyang, H. Tong, N. Umezawa, J. Cao, P. Li, Y. Bi, Y. Zhang, J. Ye, *J. Am. Chem. Soc.*, 2012, **134,** 1974.

13 T.K. Townsend, N.D. Browning, F.E. Osterloh, *ACS nano* 6 2012, 7420–7426.

14 S. Hara, H. Irie, *Appl. Catal., B*, 2012, **115,** 330.

15 A. Iwase, Y.H. Ng, Y. Ishiguro, A. Kudo, R. Amal, *J. Am. Chem. Soc.*, 2011, **133,** 11054.

16 U. Sulaeman, S. Yin, T. Sato, *Appl. Catal., B*, 2011, **102,** 286.

17 W.S. Choi, H.K. Yoo, H. Ohta, *Adv. Funct. Mater.*, 2015, **5,** 799.

18 R.B. Comes, P.V. Sushko, S.M. Heald, R.J. Colby, M.E. Bowden, S.A. Chambers, *Chem. Mater.*, 2014, **26,** 7073.

RSC Advances Accepted Manuscript

19 S. Ouyang, P. Li, H. Xu, H. Tong, L. Liu and J. Ye, *ACS Appl. Mater. Inter.*, 2014, **6,** 22726.

20 Q. Kuang, S. Yang, *Acs Appl. Mater. Inter.*, 2013, **5,** 3683.

21 L. Liu, P. Li, B. Adisak, S. Ouyang, N. Umezawa, J. Ye, R. Kodiyath, T. Tanabe, G.V. Ramesh, S. Ueda, H. Abe, *J. Mater. Chem. A*, 2014, **2,** 9875.

22 J. Guo, S. Ouyang, P. Li, Y. Zhang, T. Kako, J. Ye, *Appl. Catal., B*, 2013, **134,** 286.

23 H.W. Kang, S.N. Lim, D. Song, S.B. Park, *Int. J. Hydrogen Energ.*, 2012, **37,** 11602.

24 Y. Zhang, Q. Ji, G. Han, J. Jing, J. Shi, D. Ma, J. Sun, Y. Zhang, M. Li, X. Lang, Y. Zhang, Z. Liu, *ACS nano*, 2014, **8,** 8617.

25 Q. Xiang, J. Yu, M. Jaroniec, *J. Am. Chem. Soc.*, 2012, **134,** 6575.

26 T.K. Townsend, N.D. Browning, F.E. Osterloh, *Energ. Environ. Sci.*, 2012, **5,** 9543.

27 A.M. Schultz, P.A. Salvador, G.S. Rohrer, *Chem. Commun.*, 2012, **48,** 2012.

28 D. Sharma, S. Upadhyay, V.R. Satsangi, R. Shrivastav, U.V. Waghmare, S. Dass, *J. Phys. Chem. C*, 2014, **118,** 25320.

29 X. Guan, L. Guo, *ACS Catal.*, 2014, **4,** 3020.

30 Z. Yu, F. Qu, X. Wu, *Dalton Trans.*, 2014, **43,** 4847.

31 S.C. Hayden, N.K, Allam, M.A. El-Sayed, *J. Am. Chem. Soc.*, 2010, **132,** 14406.

32 Z. Yu, B. Yin, F. Qu, X. Wu, *Chem. Eng. J.*, 2014, **258,** 203.

33 T. An, H. Yang, G. Li, W. Song, W.J. Cooper, X. Nie, *Appl. Catal., B*, 2010, **4,** 288.

34 M. Sturini, A. Speltini, F. Maraschi, A. Profumo, L. Pretali, E.A. Irastorza,E. Fasani, A. Albini, *Appl. Catal., B*, 2012, **19,** 32.

35 C. Zhao, M. Pelaez, X. Duan, H. Deng, K. O'Shea, D. Fatta-Kassinos, D.D. Dionysiou, *Appl. Catal., B*, 2013, **134,** 83.

36 S.M. Liu, W.Y. Ding, W.P. Chai, *Physica B*, 2011, **406,** 2303.

37 H. Yu, S. Ouyang, S. Yan, Z. Li, T. Yu, Z. Zou, *J. Mater. Chem.*, 2011, **21,** 11347.

38 S. Yu, Y.H. Kim, S.Y. Lee, H.D. Song, J. Yi, Angew. *Chem. Int. Ed. Engl.*, 2014,

RSC Advances Accepted Manuscript

53, 11203.

39 J. Song, Z. Luo, D. K. Britt, H. Furukawa, O. M. Yaghi, K. I. Hardcastle, C.L. Hill, *J. Am. Chem. Soc.*, 2011, **133,** 16839.

40 M. Kong, Y.Z. Li, X. Chen, T.T. Tian, P.F. Fang, F. Zheng, X.J. Zhao, *J. Am. Chem. Soc.*, 2011, **133,** 16414.

41 G. He, C. Xing, X. Xiao, R. Hu, X. Zuo, J. Nan, *Appl. Catal., B*, 2015, **70,** 1.

42 F. Dong, Z. Zhao, T. Xiong, Z. Ni, W. Zhang, Y. Sun, W.K. Ho, *ACS Appl. Mater. Inter.*, 2013, **5,** 11392.

43 H. Xu, J. Yan, Y. Xu, Y. Song, H. Li, J. Xia, C. Huang, H. Wan, *Appl. Catal., B*, 2013, **129,** 182.

44 J. Di, J. Xia, Y. Ge, H. Li, H. Ji, H. Xu, Q. Zhang, H. Li, M. Li, *Appl. Catal., B*, 2015, **168,** 51.

45 S. Wang, D. Li, C. Sun, S. Yang, Y. Guan, H. He, *Appl. Catal., B*, 2014, **144,** 885.

46 G. Li, K.H. Wong, X. Zhang, C. Hu, J.C. Yu, R.C. Chan, P.K. Wong, *Chemosphere*, 2009, **76,** 1185.

47 Y.H. Zhang, N. Zhang, Z. R. Tang, Y. J. Xu, *ACS nano*, 2012, **6,** 9777.

48 S. Liu, N. Zhang, Z.R. Tang, Y.J. Xu, *ACS Appl. Mater. Inter.*, 2012, **4,** 6378.

49 L.Q. Ye, J.Y. Liu, C.Q. Gong, L.H. Tian, T.Y. Peng, L. Zan, *ACS Catal.*, 2012, **2,** 1677.

50 L. Ma, S. Liang, X.L. Liu, D.J. Yang, L. Zhou, Q.Q. Wang, *Adv. Funct. Mater.*, 2015, **25,** 898.

51 J. Wang, Y. Yu, L. Zhang, *Appl. Catal., B*, 2013, **136,** 112.

52 A. Fujishima, X. Zhang, D. Tryk, *Surf. Sci. Rep.*, 2008, **63,** 515.

53 J. Kim, C.W. Lee, W. Choi, *Environ. Sci. Technol.*, 2010, **44,** 6849.

RSC Advances Accepted Manuscript

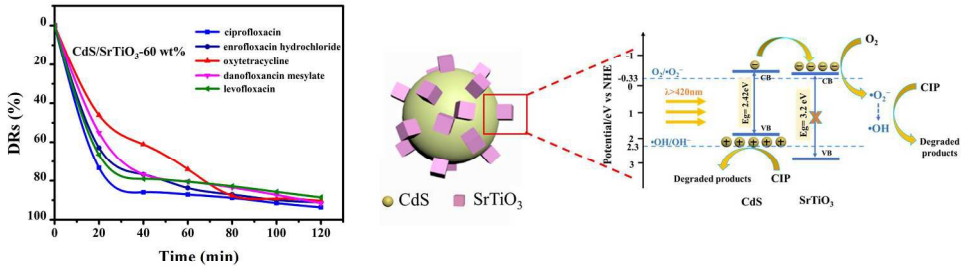

232x94mm (300 x 300 DPI)

RSC Advances Accepted Manuscript